ORIGINAL ARTICLE

lajss.org© Latin American Journal of Solids and Structures

www.lajss.org

Pressure coefficient distributions on Hyperbolic Paraboloid membranes by Numerical Fluid-Structure Interaction

Ricardo Maldonado-Ríos[a*], Mauricio Gamboa-Marrufo[a], Corneliu Cismasiu[b], Joel Alberto Moreno-Herrera[a]

[a]Engineering Faculty, Structural Engineering Group, Autonomous Univ. of Yucatán, Av. Industrias No-Contaminantes S/N, Cordemex, Mérida, Yucatán, CP 97000, Mexico. Email: a20215004@alumnos.uady.mx, mauricio.gamboa@correo.uady.mx, joel.moreno@correo.uady.mx

[b]CERIS NOVA and Department of Civil Engineering of NOVA School of Science and Technology, Caparica, 2829-516, Portugal. Email: cornel@fct.unl.pt

* Corresponding author

https://doi.org/10.1590/1679-7825/e8419

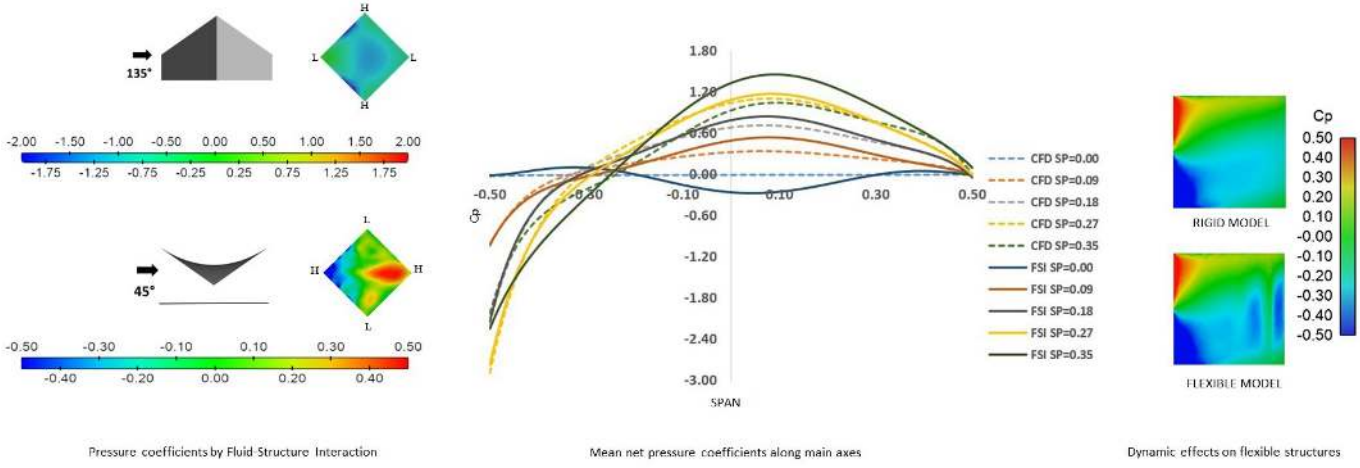
Abstract

Most studies, standards, and codes on wind pressure distributions commonly disregard the influence of the flexibility of structures. Nevertheless, in the case of tensile-membrane structures, their flexibility cannot be ignored, so this study presents the results of numerical simulations evaluating wind pressure coefficient distributions on tensile-membrane structures, accounting for fluid-structure interaction (FSI) choosing the most common geometry: the hyperbolic paraboloid. Various curvature configurations, wind incidence directions, and structural models (both open and enclosed) were analyzed. The FSI solution involves a two-way partitioned simulation between Computational Fluid Dynamics, Computational Structural Dynamics and through a coupling system that culminates in the derivation of final pressure coefficient distributions. Results indicate that pressure coefficients obtained for rigid models underestimate those obtained by the FSI methodology, which accounts for deformations altering the interaction between the fluid and membrane.

Keywords

Hyperbolic paraboloid, fluid-structure interaction, computational fluid dynamics, pressure coefficients, wind analysis, tensile membrane structures

Graphical Abstract



Received: Oct. 30, 2024. In revised form: Jan. 09, 2025. Accepted: Feb. 23, 2025. Available online: Feb. 24, 2025
https://doi.org/10.1590/1679-7825/e8419

Latin American Journal of Solids and Structures. ISSN 1679-7825. Copyright © 2025. This is an Open Access article distributed under the terms of the Creative Commons Attribution License, which permits unrestricted use, distribution, and reproduction in any medium, provided the original work is properly cited.

1 INTRODUCTION

Nowadays, the importance of wind engineering in the design of civil structures has been increased and the characterization and quantification of wind loads play a critical role. When considering irregular and flexible structures that are scarcely standardized in regulations (Forster and Mollaert, 2004; Stranghöner *et al*., 2016), such as tensile membrane structures, it reveals a domain within wind and structural engineering that demands a comprehensive and realistic approach for study. Fortunately, multiple design aspects are under exploration, including pressure analysis within a pioneering European regulation (Stranghöner *et al*., 2023).

Currently, tensile membrane structures are increasingly used to cover expansive areas like stadiums, parks, and malls. However, the evident slenderness of membranes makes these structures susceptible to substantial deformations caused by snow and water accumulation, as well as wind currents. Nevertheless, deformations induced by such loads can be stabilized or minimized through prestressing techniques (Valdés-Vázquez *et al.*, 2021; Wüchner *et al.* 2006). Additionally, as these structures are geometrically nonlinear, the imposition of prestress, boundary conditions, and initial loads plays a pivotal role in determining their shape, a factor not encountered in conventional structural design methodologies (Dutta and Ghosh, 2019). The geometric design of a membrane tensile structure involves the form-finding process, aiming to discover a self-supporting surface that minimizes stresses to solely tensile forces. Hence, the preferred arrangement involves centers of curvature positioned on opposite sides (anticlastic surface), a characteristic found in one of the most common double-curved tensile structures: the hyperbolic paraboloid, also known as hypar.

There are two primary approaches for assessing pressures exerted on structure surfaces due to wind flow loading conditions. The first method involves wind tunnel tests commonly using scaled and rigid models (Flaga *et al.*, 2018; Hincz and Gamboa-Marrufo, 2016; Sun *et al.*, 2019 and 2020). This approach typically makes use of pressure transducers to measure pressures by instrumenting these models. On the other hand, the second approach relies on computational fluid dynamics (CFD) conducted through numerical methods to solve flow equations, providing approximations of fluid behavior (De Nayer *et al.*, 2018; Pool-Blanco and Hincz, 2022; Wu *et al.*, 2008). CFD allows the extraction of significant information about fluid dynamics, including velocity gradient, turbulence effects, drag, lift, and the assessment of pressure fields on surfaces, vital in the design of structures.

Similarly, two primary challenges exist in characterizing wind loads on tensile structures. Firstly, achieving accuracy in locating and quantifying design wind loads is hindered by standards that predominantly address conventional building types. These standards often overlook tensile structures or merely account for simple geometries (CFE & INEEL, 2020; Stranghöner *et al.*, 2023). Secondly, the safety assessment of flexible structures lacks consideration for fluid-structure interaction, considering only static analyses or dynamic tests on rigid bodies.

Wind tunnel testing and CFD methodologies commonly employ rigid models to measure pressures on structures, using dimensionless coefficients. These tests vary geometrical parameters (Rizzo *et al.,* 2021a and 2022), wind directions, and surface roughness but often overlook the inherent flexibility of membrane tensile structures. Some studies acknowledge the necessity of considering aeroelasticity and advocate for numerical and experimental investigations using flexible models to estimate it (Rizzo *et al.*, 2021b). Currently, there is a rising trend in implementing CFD analysis due to advancements in computer capabilities, allowing for complex equation solving. Moreover, this tool offers the possibility of incorporating other analyses alongside fluid analysis, showcasing significant potential in addressing multiphysics problems (Colliers *et al.*, 2016).

When contemplating the flexibility of solids within fluid dynamics, the concept of fluid-structure interaction (FSI) emerges. FSI represents a phenomenon of mutual influence between a structure and a fluid, where the structure deformations alter the flow pattern. Consequently, these changes in the flow pattern lead to variations in pressures acting upon the surfaces of the structure. FSI exploration within civil engineering remains scarce. This scarcity stems from the conventional treatment of fluid forces upon rigid solid bodies such as buildings, platforms, dams, or pipes. In these cases, the interaction minimally impacts fluid behavior and structural dynamics. However, the susceptibility of tensile membranes to deformation under wind, snow, or rain loads (Liu *et al.*, 2019; Yang *et al.*, 2024) necessitates the recognition of these structures as active participants in the fluid-solid interaction process.

Numerically, FSI involves a higher computational cost compared to using CFD alone. However, FSI offers insights into pressure evolution within structures due to flow changes alongside solid deformations. This evolution of pressures enables the analysis of extreme or average pressure coefficients (Cps), crucial for designing flexible typologies not accounted for in existing codes and standards. This study incorporates numerical FSI in calculating mean pressure coefficients, focusing on a fundamental structure: the hyperbolic paraboloid. Various shape parameters related to the curvature of the structure and wind attack directions are considered for both enclosed (with perimeter walls) and open (canopy) configurations, as illustrated in Figure 1. The FSI methodology integrates CFD and computational structural dynamics (CSD) through a two-way partitioned implicit coupling scheme. The primary objective is to discern differences between applying FSI on membrane tensile structures versus traditional pressure coefficient studies using rigid models.

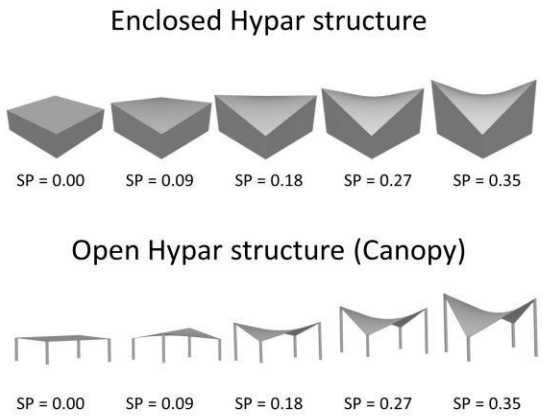


Figure 1: *Hypar with different shape parameters (SP).*

The shape parameter (SP) characterizes the curvature of the tensile structure and quantifies the variation in height between valleys and ridges in relation to the span. Specifically, for the hypar being studied, these height differences correspond to the variation in height between low corners and high corners, which define the two primary opposing curvatures. The calculation of the shape parameter is extensively outlined in Colliers *et al.* (2016). However, for this study, a symmetrical squared base was adopted to allow to express the shape parameter using equation (1), where *f* represents the maximum height difference between the crossing of the main curvatures of the tensile structure and any corner, and *L* is the horizontal distance between opposite corners:

$$SP = \frac{2f}{L} \tag{1}$$

The flat base tensile structure (SP = 0.00) maintains a uniform height of 3.25m across all four corners. In contrast, the other models showcase an increase in height for two opposing corners as the curvature rises, reaching a maximum height of 8.25m in the hypar structure with SP = 0.35. The span between the high and low corners remains constant at 10m. These specific hypar characteristics were selected to facilitate a comparison between the values published in Colliers *et al.* (2020) and obtained using CFD simulations and those assessed in this study using both CFD and FSI.

2 COMPUTATIONAL FLUID DYNAMICS

Numerical solutions for fluid-related problems typically involve a simulation tool that discretizes a finite space into control volumes with established boundary conditions. This process is executed through the utilization of the Navier-Stokes equations (2) alongside the conservation of mass or continuity equation (3) for compressible flow.

$$\frac{\partial(\rho\vec{V})}{\partial t} + \vec{V}\cdot\nabla(\rho\vec{V}) = -\nabla p + \nabla\cdot\bar{\tau} + \vec{F}_c \tag{2}$$

$$\frac{\partial\rho}{\partial t} + \nabla\cdot\rho\vec{V} = 0 \tag{3}$$

In equation (2) and (3), ρ is the density of the fluid and V its velocity vector; p refers to the pressure, τ the stress vector and F_c are the body forces in the fluid. In wind engineering, operating within the realm of subsonic velocities, wind behaves as an incompressible fluid, maintaining a constant density. Consequently, equation 3 is simplified.

For this study, the numerical model for fluid analysis was conducted using Ansys Fluent. The dimensions of the fluid domain are depicted in Figure 2, wherein the cross-section measures 64.15m at the base and 60.00m in height. Along the longitudinal axis, the domain spans 174.15m.

Upon integrating the structure model into the fluid domain, the maximum blockage percentage observed - considering the enclosed structure with SP = 0.35 is 2.97%. The inlet face of this domain is located 43.00m away from the structure and a wind velocity of 15m/s is used as input, this velocity value was chosen for comparison with the results of Colliers *et al.* (2020), who stablished Reynolds independence for rather high velocities on doubly curved membrane

structures, this was verified for this work by testing the hypar structures in a range of wind velocities from 10 to 20 m/s; it was found that the deformation had almost a linear behavior, leaving the mean Cp distribution practically unchanged. The opposite face, positioned at 174.15m from the inlet, is defined as outlet. The remaining surfaces are defined as "no-slip" condition. Furthermore, the membrane is defined as a coupling interface, using one side for the enclosed structure and two sides for the canopy case, comprising an upper and a lower interface. The SST κ-ω turbulence model was employed, because reliably predicts the flow around bluff bodies with adverse pressure gradient and massive flow separation (Simiu & Yeo, 2019). This hybrid turbulence model uses the κ-ω model for the boundary layer, while the κ-ε model is used in upper layers with low shear (Younoussi & Ettaouil, 2024). In addition, it has been established that SST κ-ω produces good results in pressure coefficients comparison with wind tunnel tests (Colliers *et al.*, 2020; Pool-Blanco & Hincz, 2022) with a lower computational expense than other complex methods (LES or DNS). Finite volumes were considered using an unstructured mesh together with prismatic elements that facilitate mesh movement (dynamic mesh) and remeshing for the FSI case. The 2.5D and spring smoothing methods have been used as remeshing and mesh adaptation techniques, respectively.

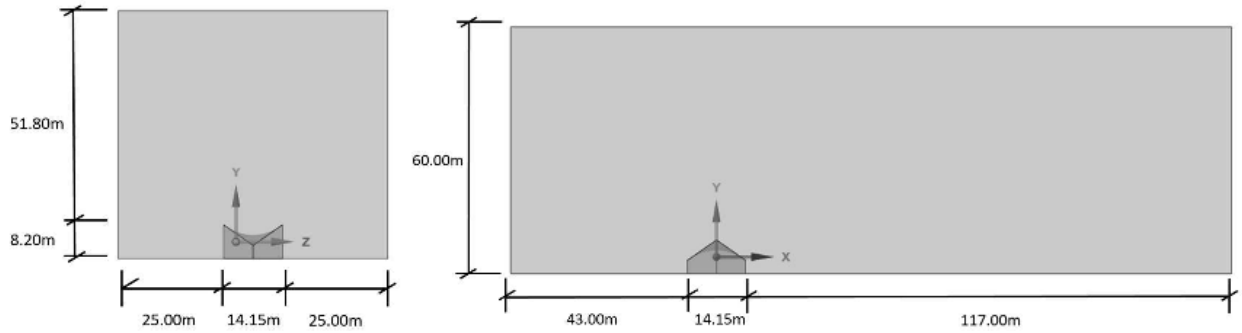


Figure 2: *Dimensions of the fluid domain.*

Studies combining experimental and numerical approaches had significantly contributed to a more comprehensive understanding of the behavior of tensile structures. An experiment involving scaled hyperbolic paraboloids conducted in wind tunnel and CFD by Colliers *et al.* (2020) aimed to explore pressure coefficient distribution, examining the influence of curvature, wind direction (45°, 90° and 135° as considered in this study), and the behavior of hypar structures with or without walls (enclosed structure or canopy). However, this experiment employed rigid models, neglecting membrane deformations, and thereby excluding any fluid-solid interaction. Consequently, this paper presents a comparative analysis of results obtained from numerical simulations using both rigid and flexible models.

To characterize the wind forces acting upon structures, pressure coefficients serve as crucial indicators. They represent the ratio between static and dynamic pressures on a surface making them dimensionless parameters. The pressure coefficient (Cp) is defined by equation (4):

$$C_p = \frac{p - p_o}{\frac{1}{2}\rho V^2} \tag{4}$$

where p is the pressure measured at the discrete point on the surface, p_0 the reference static pressure, ρ the air density and, V the unaltered wind velocity. Negative values of Cp represent suctions, while positive values correspond to pressures.

The initial step of the study involves deriving pressure coefficients for hyperbolic paraboloids while assuming a rigid membrane. This approach solely entails CFD analyses without accounting for material flexibility. The obtained results from this approximation are compared with the findings of Colliers *et al.* (2020) to ensure the consistency of results derived from the rigid model. This verification process precedes the subsequent pressure analysis involving the interaction with the flexible structure and its dynamic effects due to the consequent flow variations.

2.1 Fluid-Structure Interaction

In FSI problems, the fluid behavior is intricately linked to both the structural shape and its motion and deformation of the structure are directly influenced by the mechanical forces exerted by the fluid (Bazilevs *et al.*, 2013). In this context,

researchers laid out the foundational principles of coupling for fluid-structure interactions, exploring two distinct solution methodologies: the direct (monolithic) and the partitioned approach, which entails separate solutions for each domain (Rugonyi and Bathe, 2001). The direct solution method typically incurs significant computational expenses. Therefore, numerous studies have addressed membrane and cable tensile structures using partitioned methods (Glück *et al.*, 2003; Wu *et al.*, 2008; Wüchner *et al.*, 2006). These approaches involve either the exchange of information between the fluid domain and the structure bidirectionally (two-way simulation) or solely updating the solution of one domain based on the outcomes obtained from the other (one-way simulation). In civil engineering structures, FSI poses a challenge regarding the alignment of outcomes from two domains and, as a common practice, validating CFD results with wind tunnel experiments is frequently adopted (De Nayer *et al.*, 2018; Ortega *et al.*, 2019; Wood *et al.*, 2018). Additionally, an ongoing numerical challenge in membrane analyses revolves around wrinkling phenomena (Wang *et al.*, 2019). However, as the present study is primarily focused on deriving pressure coefficients across the surface of tensile structures considering FSI, aspects like wrinkling and the effects of pre-stress were not included in the investigation as a variable. Furthermore, prestress is previously considered to obtain the geometry during the form-finding process.

The outlined procedure for the two-way partitioned FSI simulation is illustrated in Figure 3, presenting three hierarchical iterative steps: the initial step involves the independent solution of each domain, namely CFD and CSD, separately; the subsequent step revolves around solving the coupling process, considering convergence parameters for both the fluid and structure and, lastly, the time discretization that advances linearly based on the time step of 0.005s concurrently set for both the fluid and solid components.

The numerical simulation was carried out with a coupled analysis with ANSYS 2022 R2 software and the utilization of three modules: Fluent (CFD), Mechanical (CSD), and the coupling interface (System Coupling) for exchanging results during each iteration.

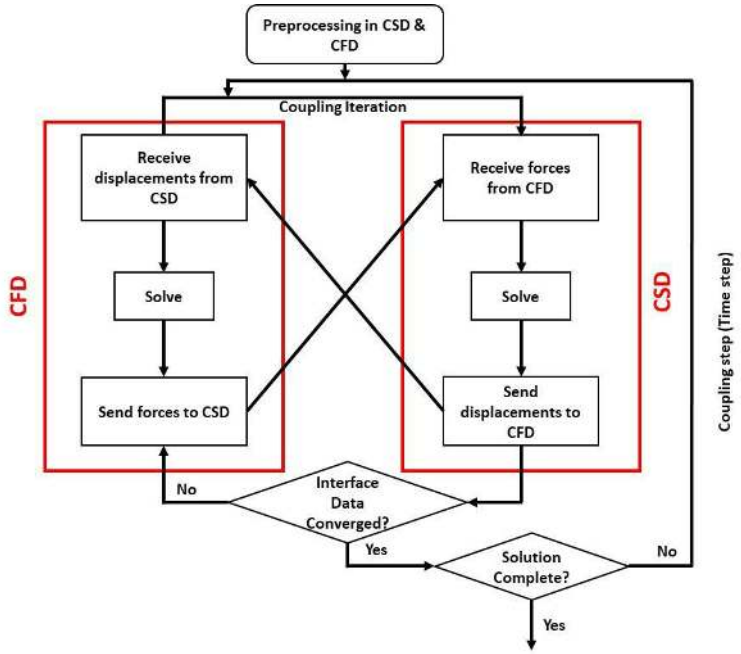


Figure 3: *Coupled 2-way methodology for FSI calculations (Badshah et al., 2020).*

In the structural domain analysis, the tensile structure thickness was maintained at 1.1mm, employing material properties characteristic of a fabric with a density of 1850kg/m^3. The Young's modulus (E) of the fabric was determined as 500kN/m for both the warp and weft directions, considering 0.3% of prestress, while the Poisson's ratio (μ) stood at 0.3. The edges of the hypars were kept fixed and rigid during the simulations for both the open and enclosed configurations, as well as the walls for the enclosed configuration, so the only surface capable of deforming was the roof. In addition, a nonlinear geometrical behavior of the membrane was considered, so that at each time step the stiffness matrix was evaluated according to the new position of the neutral axis.

The fluid domain's boundary conditions and dimensions were established based on the parameters delineated in the CFD case, as depicted in Figure 2. An unstructured mesh configuration was defined for the fluid domain, using tetrahedral control volumes. For the structural membrane, different element types were employed based on the configurations: shell elements were used for the structure with walls, while solid hexahedral elements were chosen for the open configuration.

This choice allowed for the evaluation of pressure fields on both external and internal faces of the membrane and a convergence analysis between the use of shell elements and solid elements was previously carried out. A refinement strategy was implemented at the boundary FSI to enhance precision in modeling the boundary layer behavior. Overall, each configuration consisted of between 250,000 and 510,000 finite volumes. The structural model encompassed over 2,500 elements, providing a detailed representation of the structural behavior under the influence of fluid forces.

3 RESULTS

The simulation results are presented in two sections: first, the distribution of the pressure coefficient (Cp) on the surface of the hyperbolic paraboloids obtained by equation (4) is presented, with a comparison between the rigid models and the FSI approach. Next, plots of mean Cp are shown, considering an average over a simulation period of 5 seconds (from 5s to 10s) along the two primary axes: low corner to low corner (L-L) and high corner to high corner (H-H). In the case of the canopy, mean net pressures are used, corresponding to the difference between the Cp of the upper face and the Cp of the inner face. The second section of the results shows the maximum displacements in the structure during the 10-second duration of the simulation.

These sections aim to showcase the pressure distribution across the hyperbolic paraboloids, highlighting differences between CFD on rigid models and FSI approaches, as well as demonstrating the structural behavior in terms of maximum displacements over the simulated time frame. An initial comparison, made between simulations using CFD only on rigid models and those reported in Colliers *et al.* (2020) and illustrated in Figures 4 and 5 for the wind tunnel (WT) and CFD results from the literature, respectively. Hence, Figure 5 specifically focuses on open hyperbolic paraboloids, considering two interfaces for the FSI analysis: the upper and lower surfaces, while the pressure coefficient distribution for wind tunnel tests were only available for SP = 0.09 for both enclosed and open configuration presented in Figure 4.

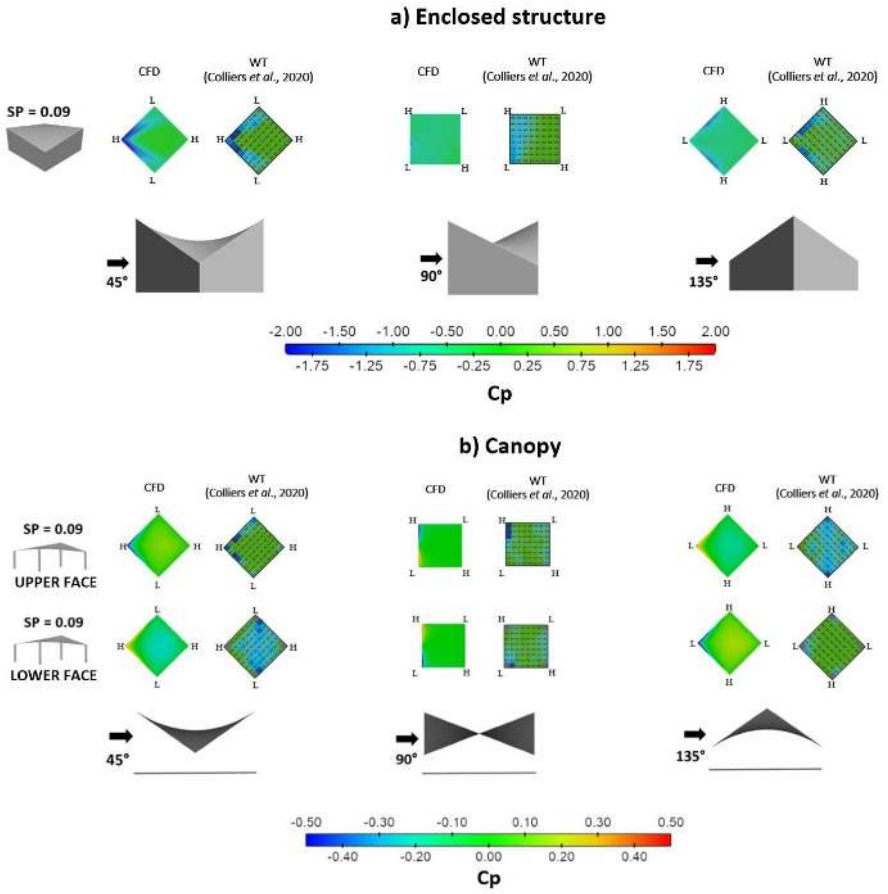


Figure 4: *CFD pressure coefficients comparison with wind tunnel results from Colliers et al. (2020).*

CFD results on rigid models versus Cp distribution from WT tests from the literature show similarities for the enclosed configuration. On the other hand, for the canopy, differences and the absence of a positive pressure zone are observed in the WT results due to discretization problems. For the canopy (Figure 5), the results of CFD simulations very

closely mirror to each other in most cases, except for SP 0.35 at 45° for the upper face at 45°and lower face at 135°, where a positive pressure zone was observed.

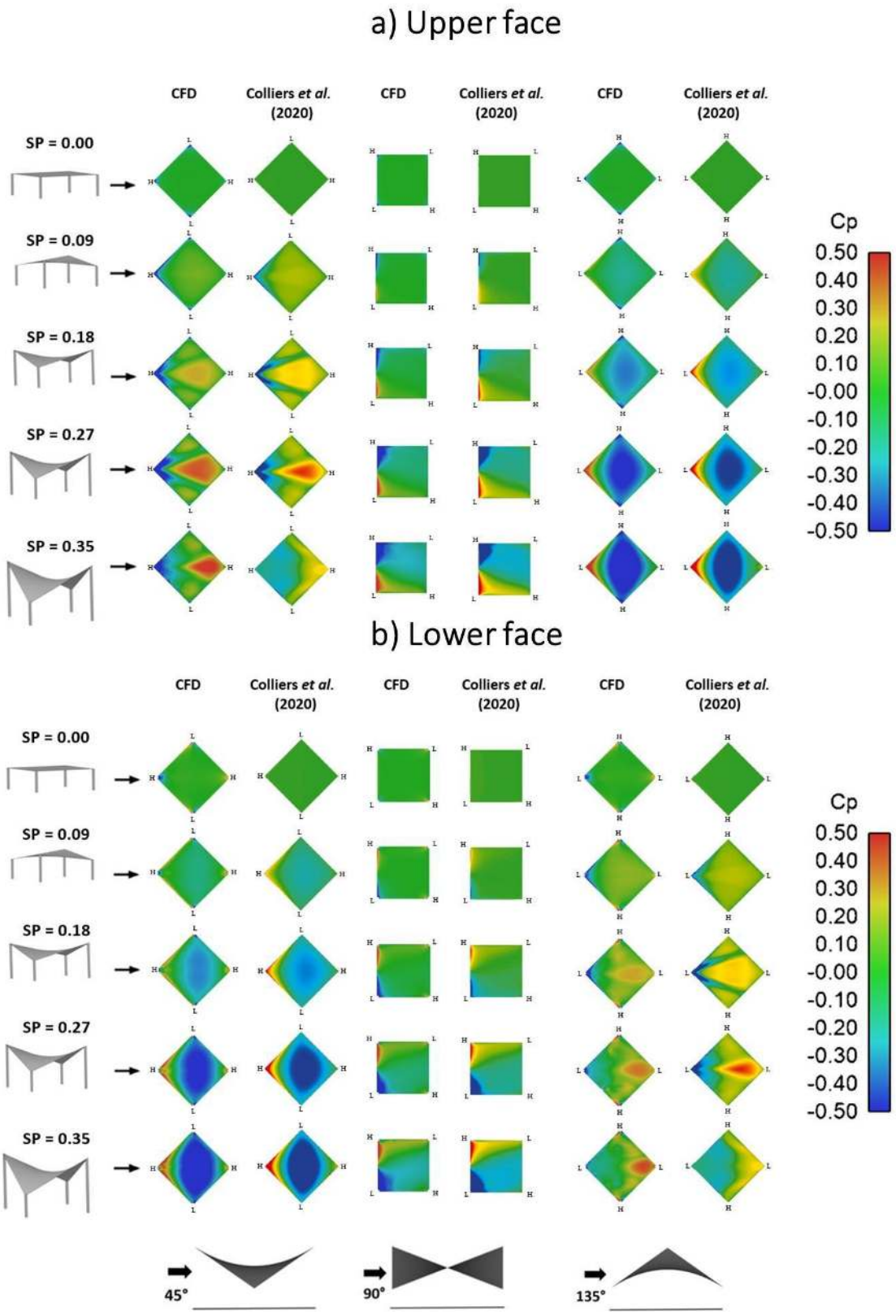


Figure 5: *Pressure coefficients comparison with Colliers et al. (2020) for upper and lower face of canopy hypar using CFD.*

3.1 Pressure coefficient distribution by FSI

From the FSI analysis of the hyperbolic paraboloid tensile structure, the pressure field over the 10-second simulation duration was acquired for various configurations encompassing different shape parameters and wind directions. Specifically focusing on the configuration with walls, Figure 6 displays the distribution of Cps obtained via CFD on rigid models and FSI at 10 seconds of simulation.

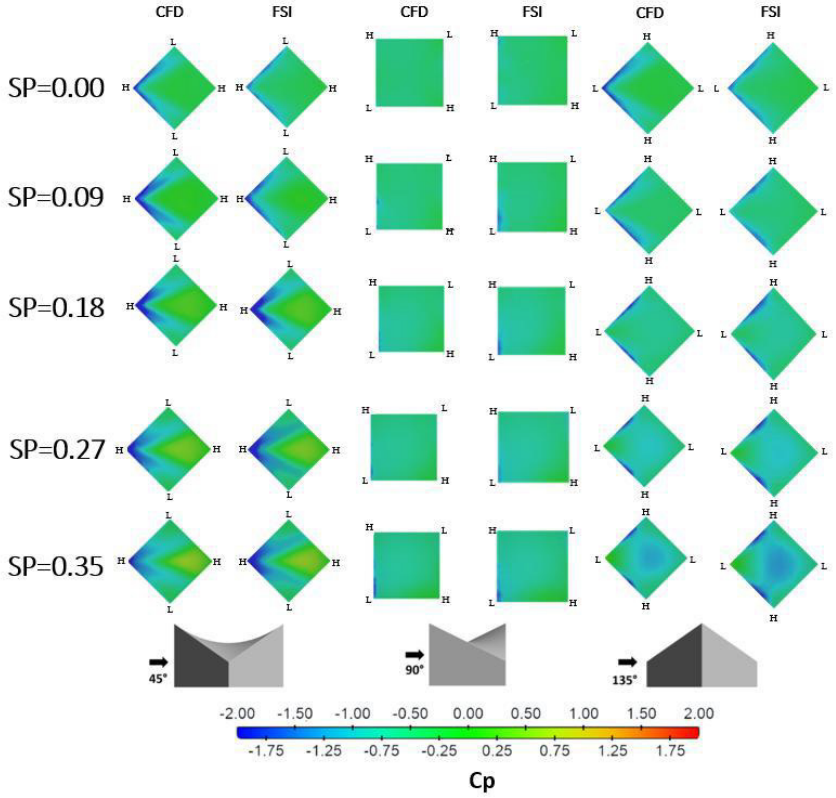


Figure 6: *Pressure coefficients distribution of enclosed hypars using CFD and FSI.*

The depicted behavior exhibits similarities between the rigid and flexible model simulations. However, as the curvature of the structure increases, noticeable disparities emerge in the suction zones as a result of the obstruction of the flow by a surface more opposed to the wind circulation (applicable in all directions). Particularly, higher absolute values are observed in the flexible structures due to flow channels generated by membrane deformations, signifying increased pressure differentials in these regions compared to the rigid model simulations.

For the open (canopy) configuration the distribution of pressure coefficients for CFD and FSI at 10s is presented in Figures 7 and 8, respectively.

The distribution of Cps for the upper face of the open hyperbolic paraboloid exhibits differences that are not present for the enclosed structure. For the highest curvature (SP 0.35) there is a drop in the Cp values on the rigid model at 45°, while the flexible model shows alternating Cps changes starting at 3.5 s. When the direction at 90° is analyzed, the flexible hypars present a transverse suction zone near the rear edge, whose values vary along with the membrane deformations. This is observed in the models with shape parameters SP = 0.18, 0.27, and 0.35 (Figure 9).

The transverse "pockets" of suction for the 90° direction are still present and sway further for SP = 0.18 and SP = 0.27, but for SP = 0.35 an extensive suction zone is defined which merges with the suction zone arising from the low windward corner (Figure 9).

Despite the extensive suction zone, the canopy with SP = 0.35 presented a stable flow for this wind direction, while the hypars with SP = 0.18 and SP = 0.27 demonstrate an alternating flow. Even with the alternating flow, the maximum and minimum values of Cp remained in the same range as those calculated on rigid models (CFD).

Regarding the flow velocity, the deformations have little effect on the overall wind behavior around the hypars, as shown in Figure 10, which compares the velocity field along the domain for the different wind directions of the enclosed hypar with SP=0.35 evaluated for both rigid and flexible models. Flow separation occurs at the same locations for both methodologies and discrepancies exist only in the leeward zone due to membrane deformations with minimal alterations in the turbulent bubble.

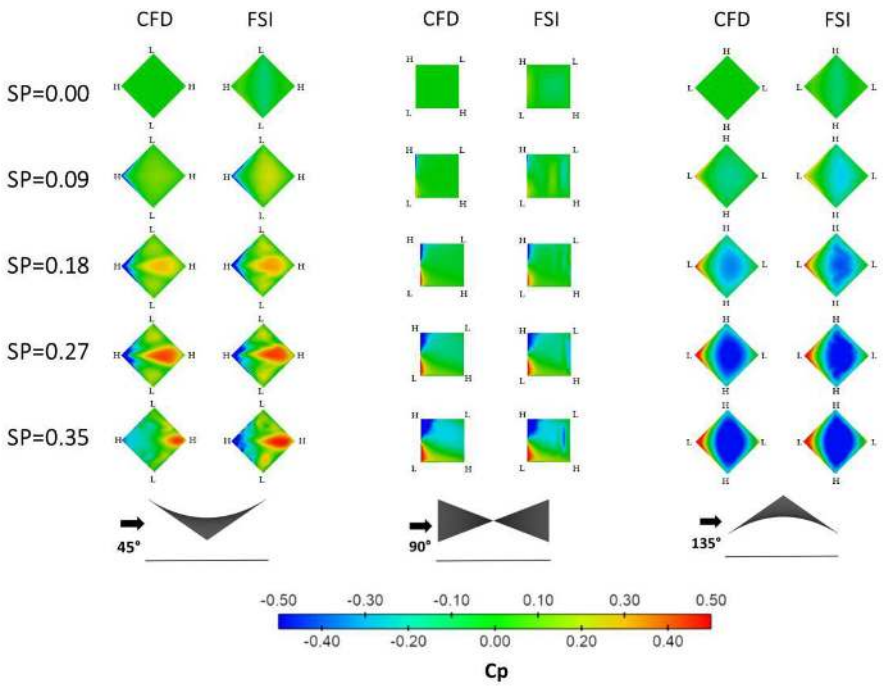


Figure 7: *Pressure coefficients distribution on upper face of open hypar (canopy).*

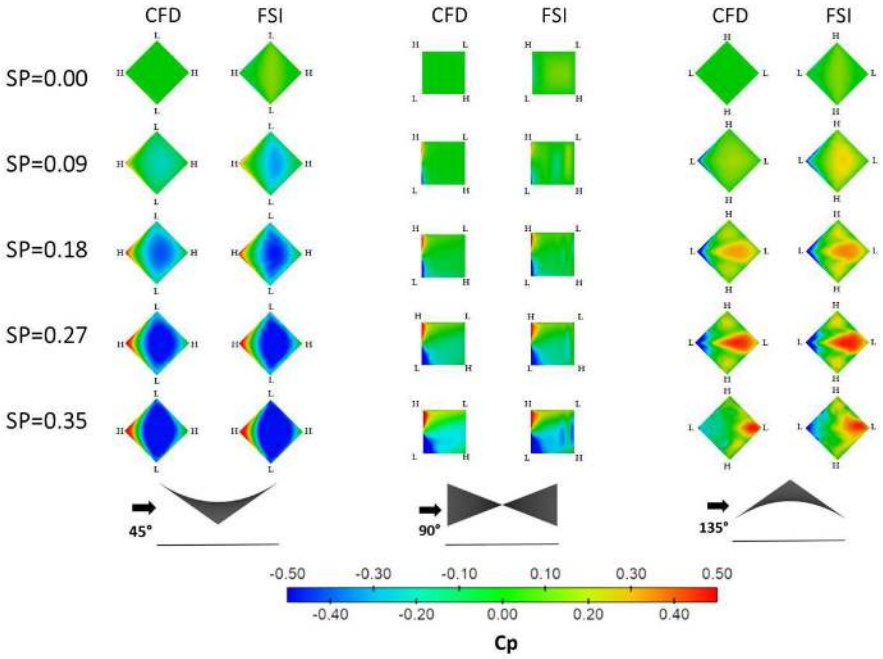


Figure 8: *Pressure coefficients distribution on lower face of open hypar (canopy).*

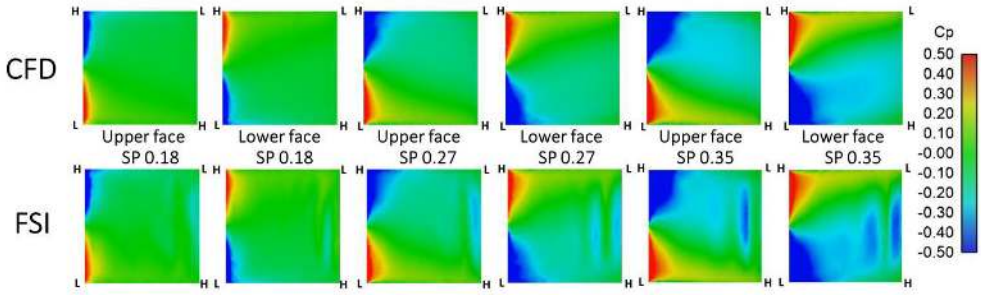


Figure 9: *Comparison of suction zones on open hypars with wind direction at 90°.*

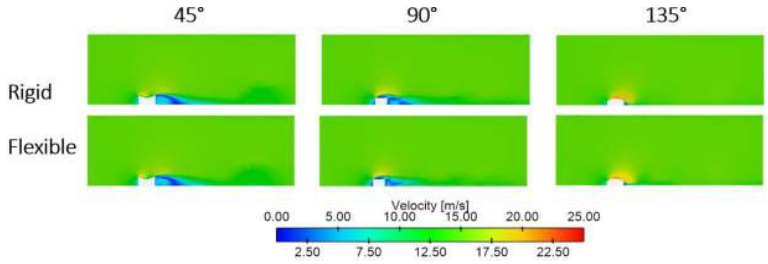


Figure 10: *Comparison of velocity map on enclosed hypar with SP=0.35 at 10s simulation time.*

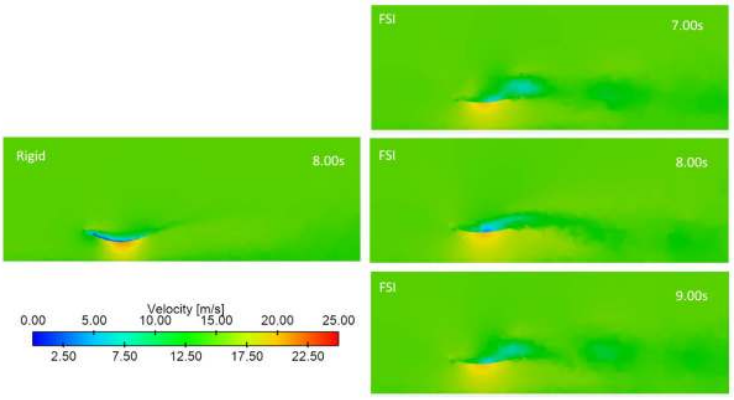
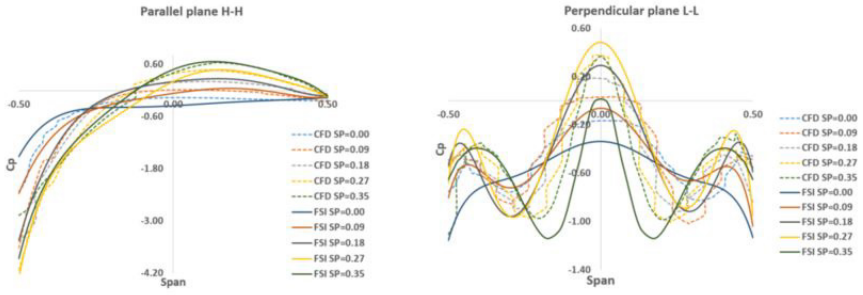
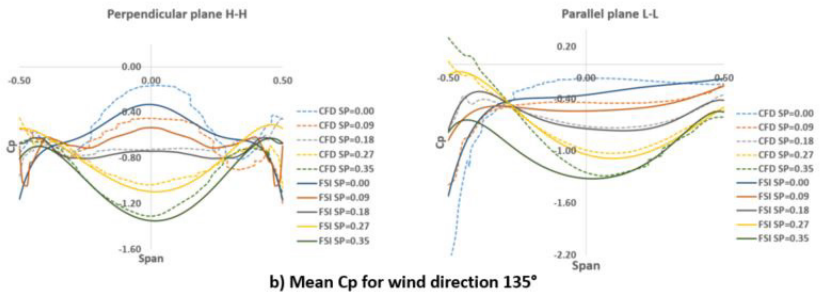


Figure 11: *Comparison of wind velocity on open hypar with SP=0.27 at 90°.*

Nevertheless, the velocity field changes for the open structure. The alternating pressure coefficients (see Figure 9) are due to the alternating flow as shown in Figure 11, where the SP=0.27 with a wind direction of 90° presents a fluctuating wind wake of between 1 and 3m/s compared to the unaltered flow when the rigid model is taken into account. In addition to an alternating effect in velocity and pressure coefficients, the deformations in the structure show a flattening of the curvature, so that the flow separation occurs smoothly and in a posterior zone of the membrane, contrary to when the rigid model is taken into account, which causes an initial suction zone. This flattening also produces a flow damping, so the wind velocities are lower for the flexible model.



a) Mean Cp for wind direction 45°

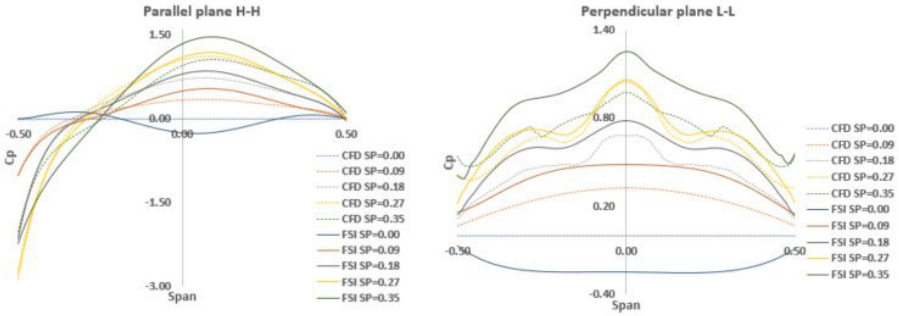


b) Mean Cp for wind direction 135°

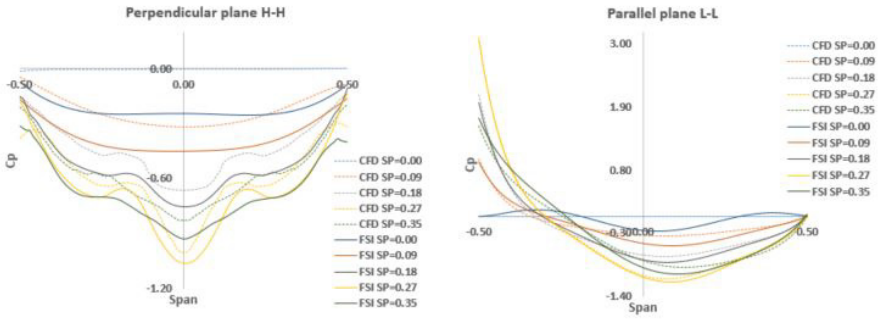
Figure 12: *Comparison of average pressure coefficients for enclosed hypar.*

The comparison of the different methods for obtaining tensile-structure Cps is shown in Figures 12 and 13, where the mean values obtained by CFD on rigid structures are compared to the mean Cps obtained by FSI. Mean Cps were evaluated from a generalized deformation stabilization (from 5s onwards). The mean pressures of the two main normalized axes are presented: from low corner to low corner (L-L) and from high corner to high corner (H-H) according to their position according to the wind direction, namely longitudinal or transverse.

As shown in Figures 12 and 13, the general trend of the curves calculated with FSI presents higher absolute values than those calculated on rigid membranes (CFD) and the maximum differences were found in the transverse axis of the canopy with 29.8% variation for SP=0.09 and 27.52% for SP=0.35 to 135° (Figure 13b), as well as 22.27% for the transverse axis from SP=0.35 to 45°. In addition, the increase in curvature implies an increase in Cp values. This statement does not apply for the canopy SP = 0.35 at 135° where the flow shedding dampens the increase in Cps, and the highest values are found for SP = 0.27 in both principal axes (Figure 13b).



a) Mean net Cp for wind direction 45°



b) Mean net Cp for wind direction 135°

Figure 13: *Comparison of mean net pressure coefficients for canopy.*

3.2 Hypar deformations due to FSI

The maximum deformations in the membrane are presented in Table 1 for the enclosed and canopy configuration. In canopy configuration, the deformations at 45° are like those at 135°, in the opposite direction. It is observed that the maximum deformations occur at low curvatures, which indicates that the double curvature configuration helps in the decrease of deformations due to wind forces, even though Cps behave in the opposite way, by increasing the magnitude of the pressure or suction as the curvature increases.

If the simulation time grows, the deformed structure stabilizes after 5 seconds without presenting important changes in its geometry, except for the tensile structures that present dynamic phenomena such as alternating vortices (for SP = 0.35 at 45° and 135° as for SP = 0.18 and SP = 0.27 at 90°) that produce an alternating change on the Cps (see Figure 9).

Figure 14 shows the displacements of the different tensile structures at the end of the simulation (10s), where the importance of the curvature in the stabilization of displacements is highlighted, damping the displacements as the curvature increases. The enclosed configuration (Figura 14a) presents deformations mainly upwards, since the obstructions of the walls cause a generalized suction in the membrane which, for the 45° direction, bifurcates as the curvature increases and a bulge appears between the sunken corridors for the larger curvatures. For the tensile structure

closed at 90°, the inflated zone corresponds to the high windward corner and, to a lesser extent, the opposite high corner. The membranes closed at 135° showed lifting in stripes in the central zone.

Table 1 Maximum hypar deformations due to FSI

Shape parameter (SP)	Wind direction	Maximum deformation (m)	
		Enclosed structure	Canopy
0.00	45°	0.41	0.26
	90°	0.42	0.24
	135°	0.41	0.26
0.09	45°	0.22	0.22
	90°	0.27	0.07
	135°	0.35	0.22
0.18	45°	0.14	0.19
	90°	0.17	0.05
	135°	0.20	0.18
0.27	45°	0.14	0.11
	90°	0.13	0.05
	135°	0.14	0.12
0.35	45°	0.14	0.09
	90°	0.11	0.05
	135°	0.10	0.08

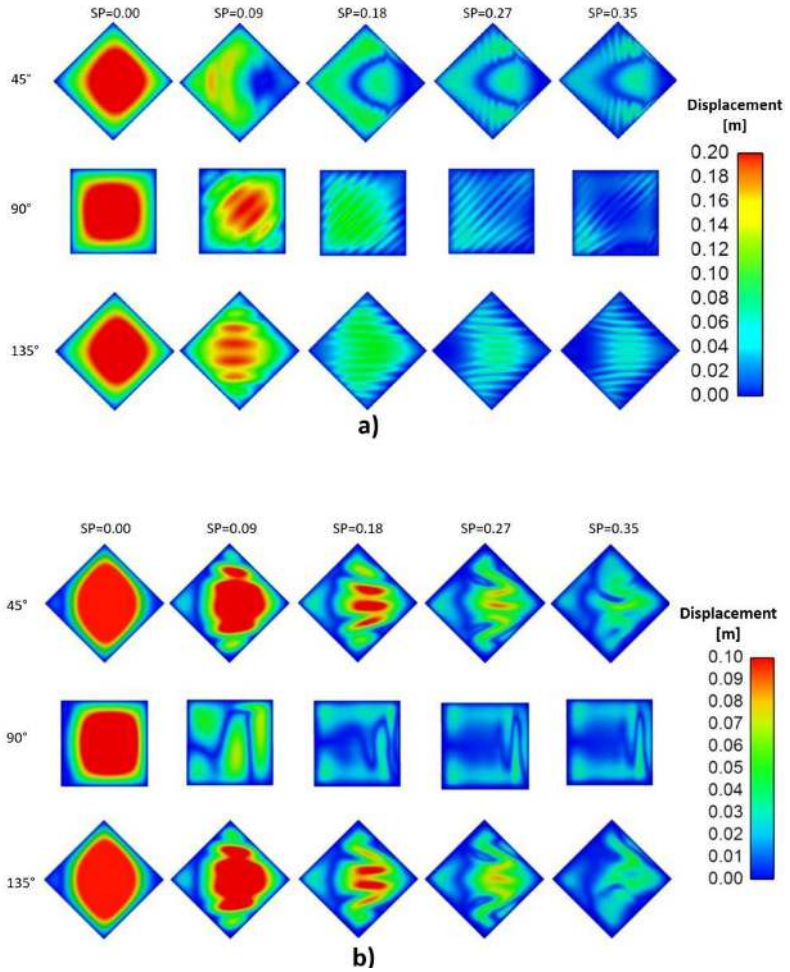


Figure 14: *Hypar displacements at 10s simulation time: a) Enclosed hypar. b) Canopy.*

On the other hand, the canopy (Figure 14b) shows both uplift and subsidence zones of lesser magnitude than the enclosed configuration. For the 45° wind direction, the membrane rises upwind, but then stabilizes until it passes the

central zone where there is subsidence; for the 135° direction, the opposite occurs as the wind initially impacts the membrane in a low corner. The 90° tensile-structures present a mixed effect, where upwind there is subsidence for the low corner and uplift for the high corner. As the curvature increases, there is an alternating flow from the central zone of the 90° open membranes as shown in Figure 9 caused by the geometry deriving a mixed flow routing.

4 CONCLUSION

The aerodynamic pressure coefficient of various configurations of full-scale hyperbolic paraboloids were determined through numerical simulations considering a constant wind velocity of 15m/s at the inlet and varying wind directions (45°, 90°, and 135°) and shape parameters (SP). These simulations were conducted using CFD and FSI methodologies.

The FSI analysis was executed using a two-way partitioned method. The pressure coefficients derived from both the CFD and FSI models exhibited similar trends. However, notable differences were observed with the FSI methodology consistently indicating higher absolute pressure values for both the open and enclosed configurations.

In addition to calculating Cps, the FSI analysis allowed the computation of membrane deformations. The analysis revealed that the most significant deformations occurred with the smallest shape parameter (SP = 0.00). Interestingly, it was observed that as the curvature increased, the deformations induced by wind flow decreased. However, Cp distribution exhibited an inverse relationship with the increasing curvature. As the curvature heightened, the area exposed to the incident wind expanded, consequently resulting in higher mean Cp values. The incident wind direction at 45° generates the highest Cps, particularly inducing significant suction values in the structure directly upwind, where the high corner interfaces with the wind. Conversely, in the valley region across the middle of the membrane, the highest-pressure values were observed.

In the FSI simulations, distinctive alternating vortices were observed, specifically noticeable due to the structure geometry in open tensile configurations. These vortices manifested for SP = 0.35 at 45° and 135°, as well as for SP = 0.27 at 90°. This dynamic behavior, unique to flexible structures, stands in contrast to methodologies focusing on rigid structures. Understanding these dynamic phenomena through FSI simulations holds significant potential in guiding the design and development of flexible structures, thereby contributing valuable insights for the refinement of standards and codes in this domain. The results obtained in this research on hyperbolic paraboloids are a second step towards a better understanding of Cp behavior in this type of structures in which taking into account deformability could be used to refine tensile membrane structures codes and standards that recommend pressure coefficient variations for hypars with different shape parameters. For pressure coefficient distributions of hypar tensile structures with rigid models, it is recommended to increase the Cp's distribution values by 30% according to the differences found between rigid and flexible methodologies to account for dynamic effects if no FSI study is available or in case a code or standard only considers static effects. And, finally, as the results for open structures at 90° show alternating flow, fatigue testing and maintenance of prestressed elements of connection and support elements must be present in the design of tensile-structures, especially when dealing with open structures with the possibility of flapping due to alternating wind effects.

Author's Contribuitions: Conceptualization, M. Gamboa-Marrufo and R. Maldonado-Ríos; Methodology, M. Gamboa-Marrufo and R. Maldonado-Ríos; Investigation, R. Maldonado-Ríos; Writing - original draft, R. Maldonado-Ríos; Writing - review & editing, M. Gamboa-Marrufo, C. Cismasiu, JA Moreno-Herrera and R. Maldonado-Ríos; Resources, M. Gamboa-Marrufo; Supervision, M. Gamboa-Marrufo, C. Cismasiu, JA Moreno-Herrera.

Editor: Marco L. Bittencourt

References

Badshah, M., Badshah, S., Jan, S. (2020). Comparison of computational fluid dynamics and fluid structure interaction models for the performance prediction of tidal current turbines. Journal of Ocean Engineering and Science, 5(2), 164–172.

Bazilevs, Y., Takizawa, K., Tezduyar, Tayfun. (2013). Computational Fluid-Structure Interaction: Methods and Applications. Wiley.

CFE & INEEL. (2020). Manual de Diseño de Obras Civiles: Capítulo C.1.4. Diseño por Viento. Comisión Federal de Electricidad e Instituto Nacional de Electricidad y Energías Limpias. México.

Colliers, J., Degroote, J., Mollaert, M., De Laet, L. (2020). Mean pressure coefficient distributions over hyperbolic paraboloid roof and canopy structures with different shape parameters in a uniform flow with very small turbulence. Engineering Structures, 205.

Colliers, J., Mollaert, M., Vierendeels, J., De Laet, L. (2016). Collating Wind Data for Doubly-curved Shapes of Tensioned Surface Structures (Round Robin Exercise 3). Procedia Engineering, 155, 152–162.

De Nayer, G., Apostolatos, A., Wood, J. N., Bletzinger, K. U., Wüchner, R., Breuer, M. (2018). Numerical studies on the instantaneous fluid–structure interaction of an air-inflated flexible membrane in turbulent flow. Journal of Fluids and Structures, 82, 577–609.

Dutta, S., Ghosh, S. (2019). Analysis and Design of Tensile Membrane Structures: Challenges and Recommendations. Practice Periodical on Structural Design and Construction, 24(3), 1–9.

Flaga, A., Kłaput, R., Kocoń, A. (2018).Wind Tunnel Tests of Wind Pressure Distributions for Four Different Tent Halls. Technical Transactions, 115(3) 91-105.

Forster, B., Mollaert, M. (2004). European Design Guide for Tensile Surface Structures. TensiNet.

Glück, M., Breuer, M., Durst, F., Halfmann, A., Rank, E. (2003). Computation of wind-induced vibrations of flexible shells and membranous structures. Journal of Fluids and Structures, 17(5), 739–765.

Hincz, K., Gamboa-Marrufo, M. (2016). Deformed Shape Wind Analysis of Tensile Membrane Structures. Journal of Structural Engineering, 142(3), 1–5.

Liu, M., Li, Q. S., Huang, S. H. (2019). Large eddy simulation of wind-driven rain effects on a large span retractable roof stadium. Journal of Wind Engineering and Industrial Aerodynamics, 195, 104009.

Ortega, E., Flores, R., Cuartero, E., Oñate, E. (2019). Efficient aeroelastic analysis of inflatable structures using enhanced potential flow aerodynamics. Journal of Fluids and Structures, 90, 230–245.

Pool-Blanco, S. J., Hincz, K. (2022). Computational Wind Engineering of a Mast-supported Tensile Structure. Periodica Polytechnica Civil Engineering, 66(1), 210–219.

Rizzo, F., Barbato, M., Sepe, V. (2021a). Shape dependence of wind pressure peak factor statistics in hyperbolic paraboloid roofs. Journal of Building Engineering, 44, 103203.

Rizzo, F., Kopp, G. A., Giaccu, G. F. (2021b). Investigation of wind-induced dynamics of a cable net roof with aeroelastic wind tunnel tests. Engineering Structures, 229(April 2020), 111569.

Rizzo, F., Sepe, V., Sabbà, M. F. (2022). Investigation of the Pressure Coefficients Correlation Field for Low-Rise Building Roofs. Applied Sciences (Switzerland), 12(21), 1–23.

Rugonyi, S., Bathe, K. J. (2001). On finite element analysis of fluid flows coupled with structural interaction. CMES - Computer Modeling in Engineering and Sciences. 2. 195-212.

Stranghöner N., Uhlemann J., Mollaert, M. (2016). Background to the Science and Policy Report for Tensile Membrane Structures. Procedia Engineering, 155, pp. 256–264.

Stranghöner, N., Uhlemann, J., Bilginoglu, F. (2023). Prospect for European guidance for the structural design of tensile membrane structures: support to the implementation, harmonisation and further development of the Eurocodes, (M. Mollaert, editor, S. Denton, editor, A. Pinto, editor, S. Dimova, editor). European Commission, Joint Research Centre, Publications Office of the European Union.

Simiu, E., Yeo, D. (2019). Wind effects on structures: Modern Structural Design for Wind. John Wiley & Sons Ltd.

Sun, X., Arjun, K., Wu, Y. (2020). Investigation on wind tunnel experiment of oval-shaped arch-supported membrane structures. Journal of Wind Engineering and Industrial Aerodynamics, 206, 104371.

Sun, X., Yu, R., Wu, Y. (2019). Investigation on wind tunnel experiments of ridge-valley tensile membrane structures. Engineering Structures, 187, 280–298.

Valdés-Vázquez, J. G., García-Soto, A. D., Chiumenti, M. (2021). Response of a double hypar fabric structure under varying wind speed using fluid-structure interaction. Latin American Journal of Solids and Structures, 18(4), 1–20.

Wang, X., Yin, L., Yang, Q. (2019). Numerical analysis of the wrinkling behavior of thin membranes. Archive of Applied Mechanics, 89(11), 2361–2380.

Wood, J. N., Breuer, M., De Nayer, G. (2018). Experimental studies on the instantaneous fluid–structure interaction of an air-inflated flexible membrane in turbulent flow. Journal of Fluids and Structures, 80, 405–440.

Wu, Y., Sun, X., Shen, S. (2008). Computation of wind-structure interaction on tension structures. Journal of Wind Engineering and Industrial Aerodynamics, 96(10–11), 2019–2032.

Wüchner, R., Kupzok, A., Bletzinger, K. U. (2006). Simulation of fluid-structure-interaction with free form membrane structures using an implicit coupling scheme with adaptive under relaxation. ECCOMAS CFD 2006: Proceedings of the European Conference on Computational Fluid Dynamics, Egmond Aan Zee, The Netherlands, 5-8, 1–17.

Yang, Q.S., Chen, F.X., Tamura, Y., Li, T., Yan, B.W. (2024). Fluid-structure interaction behaviors of tension membrane roofs by fully-coupled numerical simulation. Journal of Wind Engineering and Industrial Aerodynamics, 244, 105609.

Younoussi, S., Ettaouil, A. (2024). Calibration method of the k-ω SST turbulence model for wind turbine performance prediction near stall condition. Heliyon, 10(1).